JOURNAL OF MATERIALS SCIENCE 19 (1984) 809–814

Young's modulus of porous materials

Part 2 *Young's modulus of porous alumina with changing pore structure*

JAMES C. WANG*
State University of New York, Stony Brook, New York 11794, USA

The Young's modulus of porous alumina was determined by both sonic and bending tests. The pore structure of the specimens changes from interconnected at high porosities to disconnected at low porosities. The Young's modulus data can best be treated by the correlation proposed in Part 1 of this paper.

1. Introduction

Experimentation [1, 2] and empirical equations [3, 4] have been principally used to study the Young's modulus of porous materials. Theoretical equations are limited to isolated pores [4, 5] and are being indiscriminately used for open pores. Only recently has the subject of relating Young's modulus to the changing pore structure (from open pores to closed pores) been analysed, in Part 1 of this paper [6].

According to Part 1 the Young's modulus, E, is a complicated function of porosity, p, an approximate solution being proposed:

$$E = E_0 \exp [-(bp + cp^2)]. \quad (1)$$

where E_0 is the zero-porosity Young's modulus, and b and c are nonnegative materials constants. A higher-order term (or terms) may be included in the exponential polynomial for wider porosity ranges and for improved accuracy.

The model thus developed is highly idealized, with many assumptions. But, as shown in Part 1, most of the assumptions (e.g. simple cubic array, no-growth condition) are not essential and, furthermore, powder size can vary from specimen to specimen. Nevertheless, the assumption of monosized powder distribution within a given specimen and the assumption of the identical powder array for all specimens are still required. Unfortunately, these two required assumptions are very likely to be violated in reality because: (a) for any prolonged heating during densification, grain growth, followed by particle growth, will occur, undoubtedly altering the stacking pattern from specimen to specimen; and (b) statistically speaking, there are fast-growing as well as slow-growing particles, resulting in a nonuniform particle-size distribution within a specimen.

Therefore, it is of great interest to determine if Equation 1 can satisfactorily describe nonideal, real systems.

In this paper the Young's modulus of porous alumina will be studied, in situations where the porosity percentage not only changes, but changes also occur from interconnected to disconnected pore structure.

2. Experimental procedure and results

2.1. Materials

Porous cylindrical Al_2O_3 rods ($\simeq$ 2.2 cm diameter x 11.3 cm) were supplied by Astro Met Associate, Inc.† The density of the specimens was heavily populated around 57%, 61%, 68%, 71%, 77%, 80%, 93% and 95% of the theoretical density (TD), as shown in Fig. 2. These Al_2O_3 rods were in two batches. Following the manufacturer's nomenclature, the first batch was designated the "100 Series" and the second batch was the "300 Series". The difference between the two series was the powder shape: the 100 Series was comprised

*Present address: SCM Corporation Research Laboratory, 11000 Cedar Avenue, Cleveland, Ohio 44106, USA.
† 59 Barron Drive, Cincinnati, Ohio 44125, USA.

0022–2461/84 $03.00 + .12

of spherical powder while the 300 Series was comprised of "egg-shaped" powder.

Scanning electron microscopy (SEM) revealed that the stacking pattern was highly irregular for both series and could not be described by any known array, such as simple cubic, bcc, fcc, etc. The pores were interconnected at low densities ($\simeq$ 57% TD ~ 80% TD), while at high densities ($\simeq$ 93% TD ~ 95% TD) the pores were disconnected or only partially connected. The particle size was $\simeq 0.5\,\mu m$ for specimens with densities between 57% TD ~ 75% TD and $\simeq 1.0\,\mu m$ for specimens with densities between 75% TD ~ 82% TD. For densities greater than 90% TD, the violation of the monosize requirement was apparent, each specimen being made up by particles of various sizes: 5 ~ 10 μm for the 100 Series and 5 ~ 15 μm for the 300 Series.

Since Al_2O_3 can exist in several polymorphic forms, X-ray analysis was used to identify the crystal structure. The result indicated that the alumina was α-Al_2O_3 trigonal corundum.

2.2. Young's modulus determination

The Young's modulus was determined both dynamically and statically.

The dynamic Young's modulus was measured from the cylindrical Al_2O_3 rods by a sonic-velocity technique. A sonic-wave generator and a sonic-wave detector were attached to the opposite ends of a cylindrical rod and the sonic velocity in the axial direction was measured. Knowing the velocity, the Young's modulus was readily obtained from

$$E_s = \rho v^2 \qquad (2)$$

where ρ is the density of the alumina rod, v is the sonic velocity in the alumina and the subscript s denotes the sonic measurement.

After the sonic modulus was measured, the cylindrical Al_2O_3 rods were cut and polished into small rectangular beams ($\simeq$ 3.8 mm x 9.4 mm x 50.8 mm). The static Young's modulus was determined by three-point bending test on the rectangular beams with the supporting span being 38 mm. This geometry constitutes a large span-to-height ratio to eliminate errors introduced by a short specimen [7, 8]. The cross-head speed was 0.05 mm/min. The load and cross-head travel were recorded, a typical load-travel chart being illustrated in Fig. 1. The deflection of the specimen was obtained from the cross-head travel with a correction for machine elasticity. Knowing the

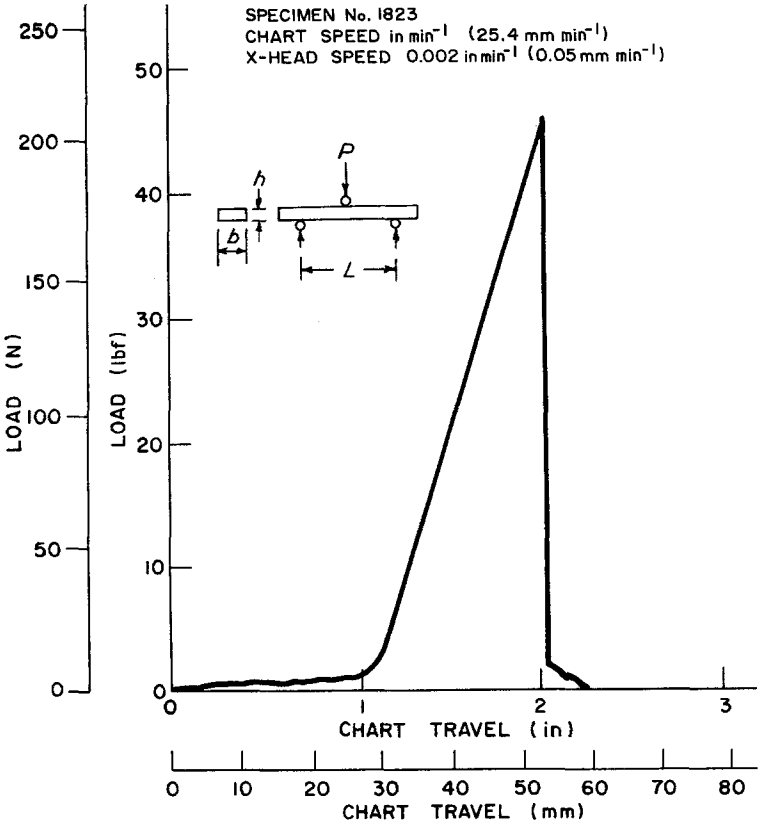

Figure 1 A typical bending-test curve.

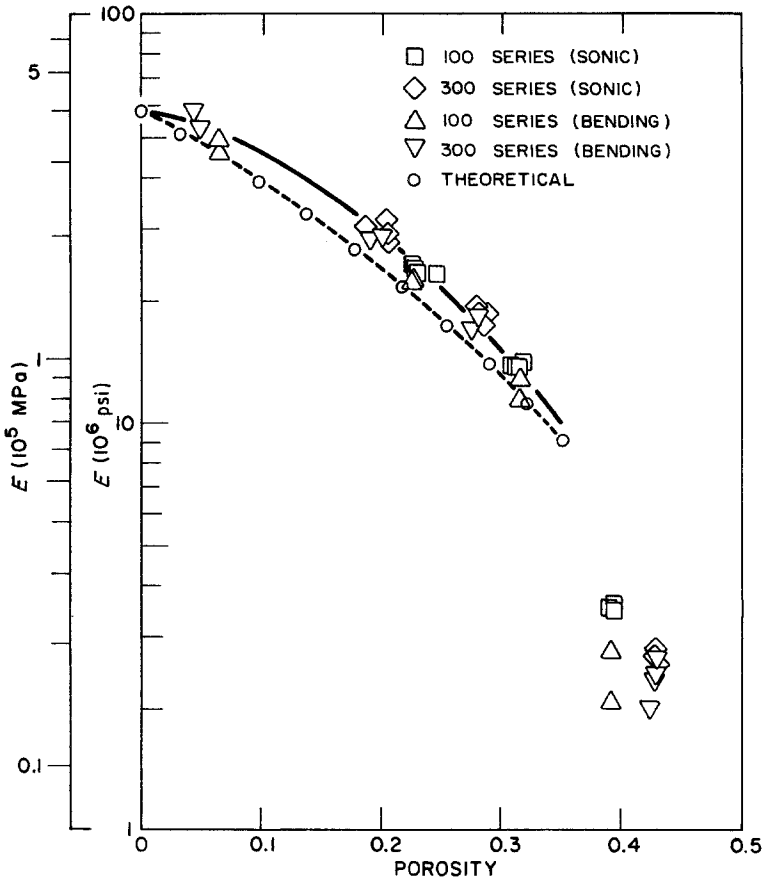

Figure 2 The Young's modulus of alumina as a function of porosity. The solid curve is Equation 4 with an applicable porosity range from zero to 0.32. The dotted curve is portion of the theoretical curve, E_2^{eff}, from Part 1 of this paper.

deflection δ and the load P, the Young's modulus can be calculated:

$$E_b = \frac{1}{4}\frac{P}{\delta}\frac{L^3}{bh^3} \tag{3}$$

where L is the supporting span, b the specimen width, h the specimen height, as shown in Fig. 1, and the subscript b denotes the bending test.

2.3. Results

The Young's modulus results from sonic measurements and bending tests are plotted in Fig. 2.

At $p \simeq 0.4$, the bending modulus has a smaller value than does the sonic modulus. This is due to the high porosity, causing local deformation and specimen damage under the loading points. The cross-head registers true deflection, as well as local deformation and damage, resulting in a decreased E_b. It should also be noted that at $p \simeq 0.4$, high porosity causes severe data scatter.

The data points suggest that the 100-Series and the 300-Series data fall on a common curve at high densities, $p = 0$ to $p \simeq 0.32$ (see Section 3.1 below). If we were to extend the curve to $p \simeq 0.32 \sim 0.4$, the curve would split into two curves with the 300-Series curve being slightly above the 100-Series curve, indicating a higher Young's modulus for the 300-Series material at low densities. This is because it is easier to close-pack spherical particles, so the 100-Series material has a higher initial packing density than does the egg-shaped 300 Series. In order for the 300-Series material to reach the packing density of the 100-Series material, a certain degree of densification is required, which causes neck formation in the 300-Series material while the 100-Series material is still only under point contact. Therefore, the 300-Series material has a more developed skeleton, hence a higher Young's modulus, at low densities. But the difference decreases in skeleton formation (i.e. the Young's modulus) between the two series with increasing density, and, hence, the data points fall on a common curve at high densities.

3. Discussion

3.1. Testing of Equation 1

From a visual inspection of Fig. 2, the data points can be connected by a smooth curve from $p = 0$ to $p = 0.32$, followed by a sharp decrease at $p \simeq 0.4$. According to Part 1, the data points between $p = 0.05$ and $p = 0.32$ can be satisfactorily described by Equation 1, a higher-power term (or terms) being required to account for the results at $p \cong 0.4$.

To test Equation 1, the results from $p = 0.05$ to $p = 0.32$ (a total of 28 data points) were analysed by a least-squares method, yielding

$$E = 58.1 \times 10^6 \exp\left[-(1.46p + 9.82p^2)\right] \text{ psi} \tag{4a}$$

or

$$E = 4.01 \times 10^5 \exp\left[-(1.46p + 9.82p^2)\right] \text{ MPa}. \tag{4b}$$

Equation 4 is plotted as a solid line in Fig. 2. The dotted curve is a portion of the theoretical curve, E_2^{eff}, from Part 1 of this paper. It can be seen from the close agreement between the theoretical curve and the experimental results that the present model is realistic. The slight difference between the solid and the dotted curves is a reflection of the difference in stacking patterns, irregular against simple cubic.

For comparison, Spriggs' equation [3] and the Hashin–Hasselman equation [9, 10] will be considered here because Spriggs' correlation is the best available empirical correlation and Hashin–Hasselman equation is the most widely used theoretical equation to date. The Spriggs' correlation

$$E = E_0 \exp(-bp) \tag{5}$$

predicts a straight-line relation between porosity and the natural logarithmic of the Young's modulus. The Hashin–Hasselman equation [9, 10]

$$E = E_0 \left[1 + \frac{Ap}{1-(A+1)p}\right] \tag{6}$$

can be rearranged into

$$\frac{1}{E} = \frac{1}{E_0} + B\frac{p}{1-p} \tag{7}$$

where $B = -(A/E_0)$. Equation 7 predicts a straight line when $1/E$ is plotted against $p/(1-p)$.

To test Spriggs' equation and the Hashin–Hasselman equation, the 28 data points from $p = 0.05$ to $p = 0.32$ are plotted, respectively, in Fig. 3 and Fig. 4. After a least-squares analysis, Spriggs' equation becomes

$$E = 75.7 \times 10^6 \exp(-5.16p) \text{ psi} \tag{8a}$$

or

$$E = 5.22 \times 10^5 \exp(-5.16p) \text{ MPa} \tag{8b}$$

and the Hashin–Hasselman equation becomes

$$\frac{1}{E} = \left(\frac{1}{242 \times 10^6} + \frac{0.138}{10^6}\frac{p}{1-p}\right) \text{psi}^{-1} \tag{9a}$$

or

$$\frac{1}{E} = \left(\frac{1}{16.7 \times 10^5} + \frac{2.002}{10^5}\frac{p}{1-p}\right) \text{MPa}^{-1} \tag{9b}$$

Equations 8 and Equations 9 are plotted, respectively, in Fig. 3 and Fig. 4. It is apparent that Equation 1 fits the experimental result (from $p = 0.05$ to $p = 0.32$) better than do Equation 5 and Equation 7.

3.2. Intrinsic Young's modulus

The intrinsic zero-porosity Young's modulus for Al_2O_3, E_0, reported by various investigators is fairly uniform in the vicinity of $58 \times 10^6 \sim 60 \times 10^6$ psi ($4.00 \times 10^5 \sim 4.14 \times 10^5$ MPa) [3, 11]. The optimum manner of obtaining E_0 is through measurements directly from zero-porosity specimen or by extrapolation from a sufficient number of low-porosity (preferably less than 5% porosity) specimens. For situations such as the present case, where only a limited number of low-porosity data are available, the extrapolation of high-porosity data to zero porosity should be avoided. Fortunately, in this study it was possible to extrapolate correctly to $E_0 = 58.1 \times 10^6$ psi (4.01×10^5 MPa). This is because Equation 1 is an excellent correlation, coupled with a large number of auxiliary data from $p \simeq 0.20$ to $p \simeq 0.32$ to compensate for the lack of high-density data. Since Spriggs' equation and the Hashin–Hasselman equation do not show good correlation, the extrapolated value of E_0 may be incorrect. It is, in fact, shown by Equations 8 and Equations 9 that Spriggs' correlation predicts E_0 to be 75.7×10^6 psi (5.22×10^5 MPa) and the Hashin–Hasselman equation predicts E_0 to be 242×10^6 psi (16.7×10^5 MPa), which are in disagreement with the value of E_0 well established in the literature.

3.3. Pore structure and porosity range

The incorrect E_0-value is not a reflection of the validity of Spriggs' or the Hashin–Hasselman equation. But rather, it means that each equation

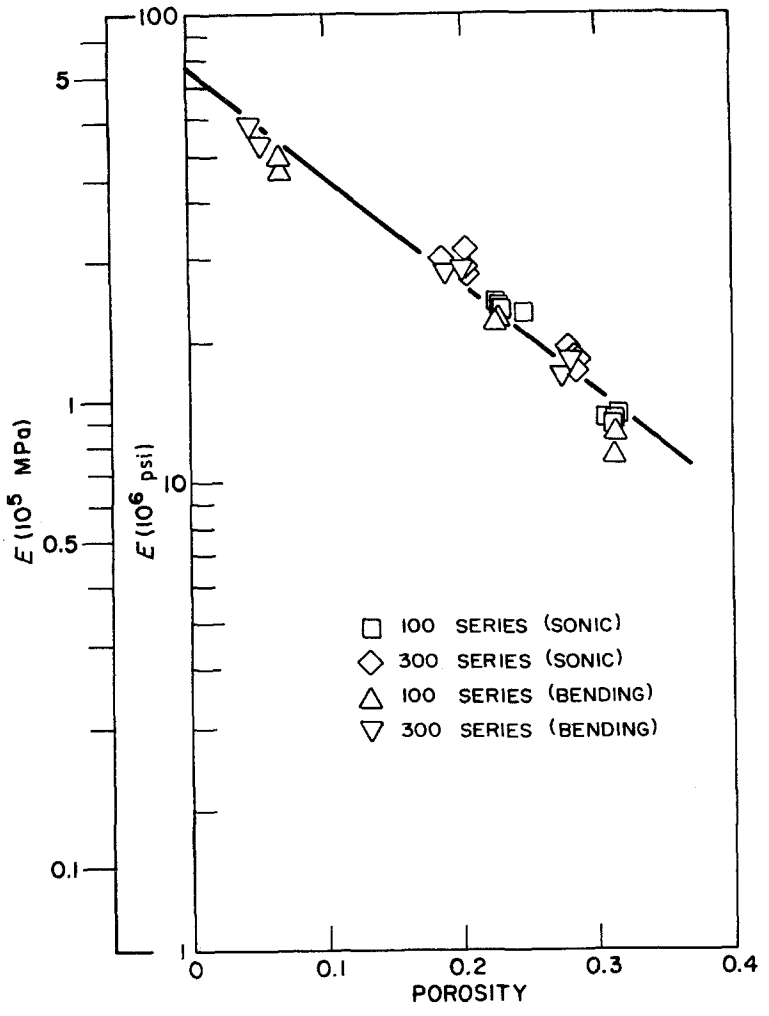

Figure 3 Spriggs' plot. A total of 28 data points (from $p = 0.05$ to $p = 0.32$) are in this plot. The solid line is obtained by least-squares analysis.

has its own intended application. For example, the Hashin–Hasselman equation is meant for isolated pores [9, 10]. The data at $p \simeq 0.20$ to $p \simeq 0.32$ correspond to interconnected pores and should not have been included in Hashin–Hasselman analysis. Since at $p \simeq 0.20$ the porosity is much less open than it is at $p \simeq 0.32$, let us assume that the pores at $p \simeq 0.20$ can be analysed by the Hashin–Hasselman equation without being too erroneous. Then let us only consider those data points from $p \simeq 0.05$ to 0.20; a least-squares analysis will result in $1/E_0 = 0.0148 \times 10^{-6}$ psi^{-1} (0.215×10^{-5} MPa^{-1}), or $E_0 = 67.5 \times 10^6$ psi (4.66×10^5 MPa), a much acceptable value. Similarly, as discussed in Part 1, Spriggs' equation is a good correlation if the porosity range is not too wide. For example, if we narrow down the porosity range to $p \lesssim 0.20$, the resulting E_0 from least-squares becomes 61.6×10^6 psi (4.25×10^5 MPa), very close to the E_0 value established in the literature.

It can be seen from the above discussion that, in selecting a suitable modulus–porosity equation, it is important that proper consideration be given to the pore structure and the porosity range in question. The Hashin–Hasselman equation is for closed pores. Spriggs' equation is for both open and closed pores and for relatively small porosity ranges. The relation proposed in Part 1 of this paper is for both open and closed pores over a wider porosity range, and is capable of treating the transition of the pore structure from open to closed.

3.4. Nonspherical particles

It is interesting to find that the theoretical analysis of Part 1, which was based on spherical particles, applies not only to the spherical 100 Series, but

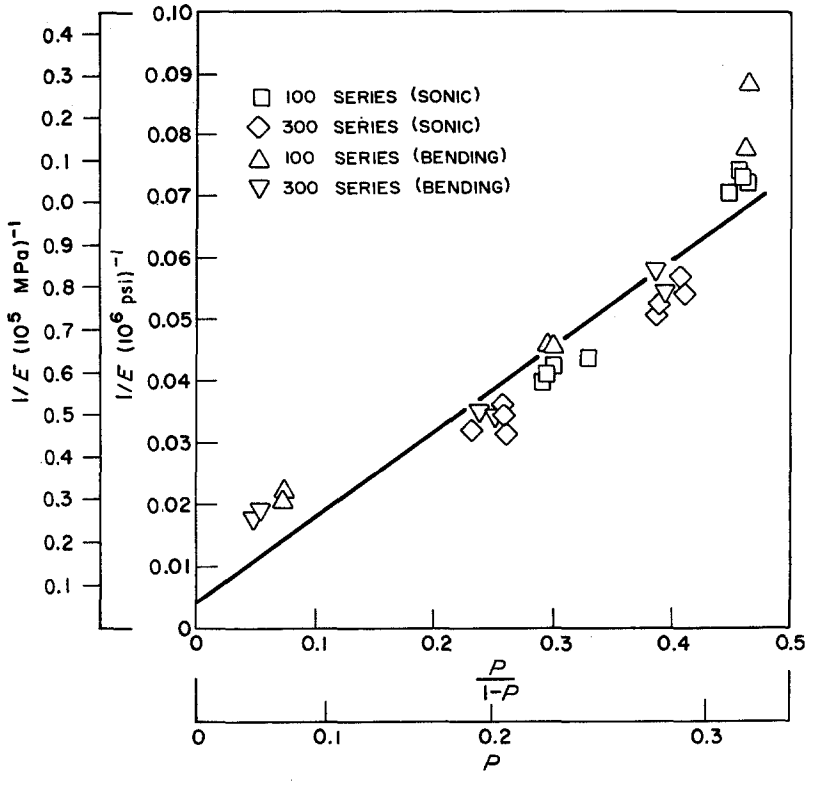

Figure 4 Hashin–Hasselman plot. A total of 28 data points (from $p = 0.05$ to $p = 0.32$) are in this plot. The solid line is obtained by least-squares analysis.

also to the nonspherical 300 Series. This is because of the fact that densification leads to a deviation from the particle's original shape, converting it into a polyhedron. The difference between a spherical particle and a nonspherical particle becomes less and less distinguishable as both approach polyhedrons during densification. Therefore, Equation 1 can also be applied to nonspherical particles.

4. Summary

The Young's modulus was determined by sonic-velocity measurements and bending tests on two batches of porous Al_2O_3. The first batch was comprised of spherical powder and the second was made of egg-shaped powder. The pore structure is interconnected at low densities and becomes disconnected at high densities. The current data can be described by the model proposed in Part 1 of this study. The zero-porosity Young's modulus E_0 is determined to be 58.1×10^6 psi (4.01×10^5 MPa), in good agreement with that reported in the literature.

Acknowledgements

The author would like to express his sincere thanks to Dr Herbert Herman and Dr Franklin Wang for their valuable suggestions and to the late Dr Allan Auskern for his indispensable help during the course of this study. The author would also like to thank Brookhaven National Laboratory for the use of laboratory facilities.

References

1. R. E. FRYXELL and B. A. CHANDLER, *J. Am. Ceram. Soc.* 47 (1964) 283.
2. G. W. HOLLENBERG and G. WALTHER, *J. Am. Ceram. Soc.* 63 (1980) 610.
3. R. SPRIGGS, *J. Am. Ceram. Soc.* 44 (1961) 628.
4. J. B. WACHTMAN, "Mechanical and Thermal Properties of Ceramics", NBS SP No. 303 (1969) 139.
5. R. W. RICE, "Treatise on Materials Science and Technology", Vol. 11, edited by R. K. McCrone, (Academic Press, 1977) p. 199.
6. To be published (Part 1 of this paper).
7. W. H. DUCKWORTH, *J. Am. Ceram. Soc.* 34 (1951) 1.
8. L. H. WILIGAN, *J. Am. Ceram. Soc.* 36 (1953) 159.
9. Z. HASHIN, *J. Appl. Mech.* 29 (1962) 143.
10. D. P. HASSELMAN, *J. Am. Chem. Soc.* 45 (1962) 452.
11. J. B. WACHTMAN, W. E. TEFFER, D. G. LAM and R. P. STINCHFIELD, *J. Res. NBS* 64A (1960) 213; *Ceram. Abstr.* (1961) June 152C.

Received 14 June
and accepted 28 June 1983